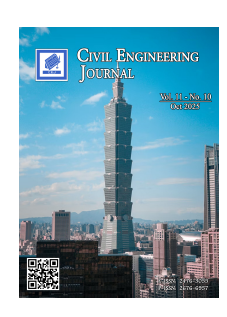


Civil Engineering Journal

(E-ISSN: 2476-3055; ISSN: 2676-6957)

Vol. 11, No. 10, October, 2025



Study on Shear Behavior of Reinforced Concrete Beams Confined with Reinforcing Meshes

Bashar F. Abdulkareem ¹*, Teghreed H. Ibrahim ², Hussein K. Mohammed ³, Abbas A. Allawi ²

Department of Reconstruction and Projects, University of Baghdad, Baghdad 17001, Iraq.
 Department of Civil Engineering, University of Baghdad, Baghdad 10071, Iraq.
 Iraqi Ministry of Higher Education and Scientific Research, Baghdad, Iraq.

Received 01 June 2025; Revised 15 September 2025; Accepted 21 September 2025; Published 01 October 2025

Abstract

This study reveals the results of a numerical simulation performed using the ABAQUS/CAE finite element program. The study aimed to provide a simulation model that can forecast the shear behavior of reinforced concrete beams confined with reinforcing meshes. Limited numerical studies have been conducted using geogrid or FRP mesh as shear reinforcement, with limited representation accuracy and limited material quality. The results were compared to published experimental findings in the literature. The finding of the finite element model and the experimental results were highly comparable; consequently, the model was determined to be valid. Following this, the domain of numerical analyses was broadened to include the investigation of many aspects, like the material of reinforcement mesh, the angle of inclination of mesh strip, and the number of mesh strips. The results show that the inclined strip beams gave ultimate loads greater than the beams with vertical strips, where the ultimate load for beams with inclined strips was higher than that for beams with vertical strips by 5.6, 2.5, and 9.4% for beams with geogrid, geotextile, and GFRP mesh, respectively. The smaller the strip width and the larger the number, the better. Beams with inclined strips (45°) gave higher ductility indexes than similar beams with vertical strips. Beams with six strips (width of 50 mm) gave higher ductility indexes than similar beams with four strips (width of 75 mm).

Keywords: Shear Strength; Concrete Beams; Geogrid Mesh; GFRP Mesh; Ductility; ABAQUS.

1. Introduction

Recently, a number of researchers have improved reinforced concrete structures by using geosynthetic materials, also known as geogrids, which are known for their exceptional flexibility and produce better results. Ferrocement laminates made of fiber-reinforced polymer (FRP) mesh, geogrid, or welded wire have shown a number of benefits. Ferrocement exhibits exceptional durability, ductility, and toughness. Moreover, ferrocement may be easily moulded into various forms to conform to the shapes of the components requiring repair [1-4]. The corrosion of steel significantly jeopardizes the durability of traditional reinforced concrete (RC) constructions. An effective method for reducing steel corrosion is replacing steel reinforcing bars in concrete with fiber-reinforced polymer (FRP) composites [5-7].

Globally, the enhancement or retrofitting of reinforced concrete structures has been a critical concern for many decades. In the case of a powerful column, a thin beam configuration, flexural failure is preferred over shear failure of

^{*} Corresponding author: b.faisal1101@coeng.uobaghdad.edu.iq





© 2025 by the authors. Licensee C.E.J, Tehran, Iran. This article is an open access article distributed under the terms and conditions of the Creative Commons Attribution (CC-BY) license (http://creativecommons.org/licenses/by/4.0/).

the reinforced concrete beam, which is achieved by enhancing shear resistance capability. In the instance of shear failure in a reinforced concrete beam, disastrous failure happens without any prior warning. Shear deficit in reinforced concrete structures may arise from elevated service loads, insufficient shear reinforcement owing to corrosion, and mistakes in construction. Shear failure is comparatively more unpleasant and more perilous than flexural failure because of its brittle characteristics [8, 9].

Tetta et al. (2015) [10] carried out an experimental study on the shear enhancement of rectangular RC beams utilizing modern composite components. The principal variables investigated in this study encompass: (a) the strengthening method, FRP jacketing, and including textile-reinforced mortar (TRM) wrapping; (b) the configuration of reinforcement, including bonding on side, U-wrapping, and complete wrapping; and (c) the quantity of reinforcement layers. A total of 14 reinforced concrete beams were fabricated and subjected to bending loads during testing. One beam was unstrengthened and functioned as the control beam; eight beams were reinforced with TRM jacketing, while the remaining five were enhanced with FRP jacketing. It is founded that TRM is frequently less successfully than FRP in increasing the shear capacity of concrete; however, the number of layers and the strengthening configuration determine how well it works..

Tetta et al. (2016) [11] carried out a study on the performance of TRM jacketing for shear strengthening of T-section RC beams, highlighting the effectiveness of a novel end-anchorage method that uses textile-based anchoring. This research investigates the following variables: (a) the use of textile-based anchors as the end-anchorage system for TRM U-jackets; (b) the number of TRM layers; (c) the textile types (material, shape). Eleven RC T-beams were made up and tested under supported conditions. The findings showed that (a) the implementation of textile-based anchors greatly improves the efficacy of TRM U-jackets; (b) enhancing the number of layers in not-anchored jackets leads to proportional rise in shear strength while concurrently modifying the failure mode; and (c) employing different textile forms with similar reinforcement ratios in not-anchored jackets yields virtually equivalent increases in full capacity. Majumder et al. (2018) [12] studied the effect of geogrid for shear strengthening in shear RC beams using experimental results. RC beam samples exhibiting shear lack were internally reinforced with a geogrid layer. The experimental results showed that the capacity of the beam with geogrid increased by 24.35% compared to the control beam. A significant increase in ductility is observed in the strengthened beam compared to the control one. The failure mode changed from flexural-shear to flexural following the confinement of the strengthened concrete beam with geogrid.

Yalciner et al. (2018) [13] tested the effect of many confinement methods, including traditional shear reinforcement ties and geo-grid confinement of full-scale RC beams. Fifteen specimens tested under the impact of monotonic testing under different conditions. The effect of plastic fibers was analyzed using two unique confinement methods. The test results showed that the use of geo-grids as stirrups did not show a favourable alignment with the performance provided by conventional stirrups. Erfan & El-Sayed (2019) [14] presented a novel method about the shear performance of box RC beams reinforced with combined textiles. Wire mesh and stirrups were employed as additional stirrups for this reason. Seven concrete beams with a box section were evaluated. Beams reinforced with tensile wire mesh demonstrated an increase in load-carrying capacity, shear strength, and deflection compared to beams utilizing fiber-glass wire mesh rather than stirrups.

Zhang et al. (2019) [15] presented the findings of static load tests carried out on ten RC beams, involving eight samples strengthened in shear using textile reinforced geopolymer mortar (TRGM), one sample strengthened with epoxy and textile, and another un-strengthened sample. The impact of the shape of the textile, the number of layers, the textile configuration, the adhesive type, and the fastening techniques using steel strips on the shear strength of reinforced beams was analysed. According to test results, one layer and two layers of TRGM reinforcement improve shear performance by 47.0% and 106.0%, respectively, as compared to the reference beam. The shear strength can be enhanced by 15.0–21.0% by the use of steel strip anchoring.

Li et al. (2020) [16] proposed a novel type of FRP shear reinforcement for RC beams. Instead of using traditional stirrups, the beams are reinforced using carbon fiber-reinforced polymer mesh (CFRP-MF). The shear behavior of fifteen beams reinforced with CFRP-MF structure, either with or without stirrups as reference samples, is examined in this study. The shear span-depth ratios (a/d of 1, 2.5, and 3.5) and the shear ratios of reinforcement of CFRP-MF composites (0.036%, 0.067%, and 0.097%) compose the study's parameters. According to the experimental results, concrete beams strengthened in shear employing the CFRP-MF arrangement exhibit shear properties that are comparable to those of the corresponding RC control beams strengthened with steel stirrups, especially with regard to the shear strength and total load-deflection relations.

Al-Bazoon et al. (2022) [17] examined the application of wire mesh—epoxy composite (WMEC) for shear-reinforced RC beams, emphasizing the following factors: (1) the existence of shear reinforcement within the shear span; (2) the kind of strengthening method utilized (vertical U strip, U-jacketing, or sloping strip); and (3) the quantity of layers of

wire mesh implemented (6 or 3). Nine RC beams were subjected to static loading tests. The results indicated that all types of WMEC improved shear capacity. Of the three structural-strengthening procedures, the continuous U-jacket method had the most significant impact, enhancing shear capacity by 33.40% to 95.90% and improving the shear ductility factor by 23.0% compared to the control beam.

The shear behavior of RC beams strengthened with CFRP-MF as shear stirrups for RC parts was experimentally studied by Li et al. [18]. A unique CFRP-MF interlaced in parallel and vertical orientations was investigated as a substitute for traditional shear reinforcing methods. Three RC beams were constructed as controls to evaluate the shear behavior of the innovative composite beams, and six CFRP-MF beams were used as shear reinforcements. The research variables were the CFRP-MF shape and the overlapping circumstance at the crossing point. According to the test findings, these innovative composite beams have ductility and shear capabilities comparable to those of conventional concrete beams with steel stirrups.

Yang & Huang (2024) [19] presented experimentally results about four RC beams. One beam operated as an unreinforced reference sample, in contrast, three were exposed to various shear strengthening techniques: polymer-modified mortar (PMM), engineered cementitious composites (ECC), and CFRP grid-reinforced ECC matrix composite layers (FGREM). The study included load-deflection relations and failure mechanisms. The test findings were replicated using numerical analysis. Important results indicate that ECC, functioning as a matrix, effectively decreases concentrated interfacial bonding strains, hence averting debonding failure. The FGREM improved beam demonstrated a failure mode marked by the splitting of the concrete cover, resulting in a significant 124.0% improvement in shear strength. The proposed finite element model, integrating interfacial performance, precisely replicated the performance of all samples.

Hashemi et al. (2024) [20] presented an experimental research to examine the behavior of glass fiber reinforced geogrid (GFRG) mesh in concrete. For this research, forty two similar cylindrical concrete measuring 15 cm in diameter and 30 cm in height were fabricated. The samples were generated in both unconfined and confined conditions, using GFRG mesh confined concrete. The samples showed varying hoop layer counts of 1, 1.5, and 2 layers. The results showed that the using GFRG mesh with concrete results in a small reduction of around 3% in confinement strength at 28 days. Ductility and post-cracking performance are enhanced, resulting in a 20.0% enhacement in energy absorption.

Guo et al. (2024) [21] examined the numerical shear response of RC beams enhanced with an FRP grid. The criteria included the shear span ratio, the grade of the concrete, the tensile strength of engineered cementitious composites (ECCs), the cross-sectional area of the FRP grid, the thickness of the ECC cover, and the number of layers of the FRP grid. A calculating method was finally devised to predict shear capacity, which was corroborated by findings from FE models and experimental results. The results showed that the FRP grids alleviated the concentration of stresses inside the flexural shear region, hence avoiding early concrete cracking. The maximum load was augmented by 8.059% when the ECC's tension strength escalated from 4.0 MPa to 10.0 MPa. Furthermore, augmenting the cover thickness from 0.8 cm to 2 cm resulted in a 14.42% rise in the peak load. This research presents a mathematical procedure that precisely estimates the shear capability of the inclined section of reinforced concrete beams.

Huang et al. (2024) [22] examined the shear performance of RC beams strengthened with CFRP rods and grids as main reinforcements and stirrups, utilizing experimental and numerical methods. Five RC beams were subjected to a monotonous load and exhibited shear failure as anticipated. The test factors, comprising grid size and stirrup ratio, were examined to analyze the interaction between the grid and concrete, in addition to the impact of the vertical and horizontal grid fibers. The study determined that decreasing the grid size while maintaining a fixed stirrup ratio might significantly enhance the distribution of stresses within the fibers of the grids and the shear capability of the sample. The grid size significantly influenced the shear capability of beams when the stirrup ratio varied within a narrow range. The horizontal fibers of the grid exerted anchoring impacts on the vertical fibers. They immediately transmitted the tension stress from the concrete at both the bottom and top of the sample. In finite element analyses, the layer of fiber composites was utilized to represent the CFRP grid. The strain evolution of the grid and the load midspan deflection of beams in the finite element model exhibited strong concordance with the experimental results. During the analysis of parameters, the grid arrangement with the horizontal fiber positioned in the central or top region was advised.

Kirthiga & Elavenil (2024) [23] examined the utilization of knitted alkali-resistant glass fabric reinforced cementitious matrix (AR-GFRCM) to enhance the performance of reinforced concrete (RC) beams lacking in flexural and shear strength. It analyzes the effects of pre-cracking reinforced concrete beams at damage levels of 50%, 75%, and 100% with fabric layers of 1, 2, or 3. The testing findings indicated that all reinforced beams had

an enhancement in failure load at different pre-cracking levels, with additional strength gains reported upon the incorporation of additional layers of textiles. A study was conducted to validate the precision of the shear strength of the reinforced beams as anticipated by ACI 549.4R-13 recommendations. The analytical investigation validated the superior flexibility and high level of accuracy of the expected outcomes, demonstrating the efficacy of AR-GFRCM in reinforcing RC structures.

Zhang & Lan (2025) [24] examined the impact of multiple factors on the shear behavior of reinforced concrete beams augmented with FRP grids–polymer cement mortar (PCM) combination, and to develop a more precise equation for the shear performance of these beams, the following tasks were undertaken in this study: Initially, the numerical simulation of the FRP grid–PCM combination reinforced concrete beams model is conducted using ABAQUS and is contrasted with the experimental findings to validate the accuracy of the model. A calculation method for the shear strength of RC beams reinforced with an FRP grid–PCM combination is provided, contingent upon the most efficient strain of the FRP grid to measure its actual shear effect. The findings indicate that the model developed in this study can accurately replicate the shear performance of the tested beams; furthermore, the influence of the quantity of the shear span ratio, FRP grid, and the concrete capacity is more pronounced. The theoretical conclusions of the equation align well with the gathered experimental data.

The study aimed to provide a simulation model that can estimate the shear behavior of RC beams confined with reinforcing meshes. Limited numerical studies have been conducted using geogrid or FRP mesh as shear reinforcement, with limited representation accuracy and limited material quality. There are two sections to this research: the first is to verify the validity of the simulation model, and the second is a comparative study between the types, number, and direction of the reinforcement networks, using this model.

2. Research Significance

Limited numerical studies have been conducted utilizing geogrid or FRP mesh as shear reinforcement, constrained by the flexural behavior of the RC beams. The study aimed to provide a simulation model that can estimate the shear behavior of RC beams confined with reinforcing meshes. Figure 1 illustrates the flowchart for the research approach.

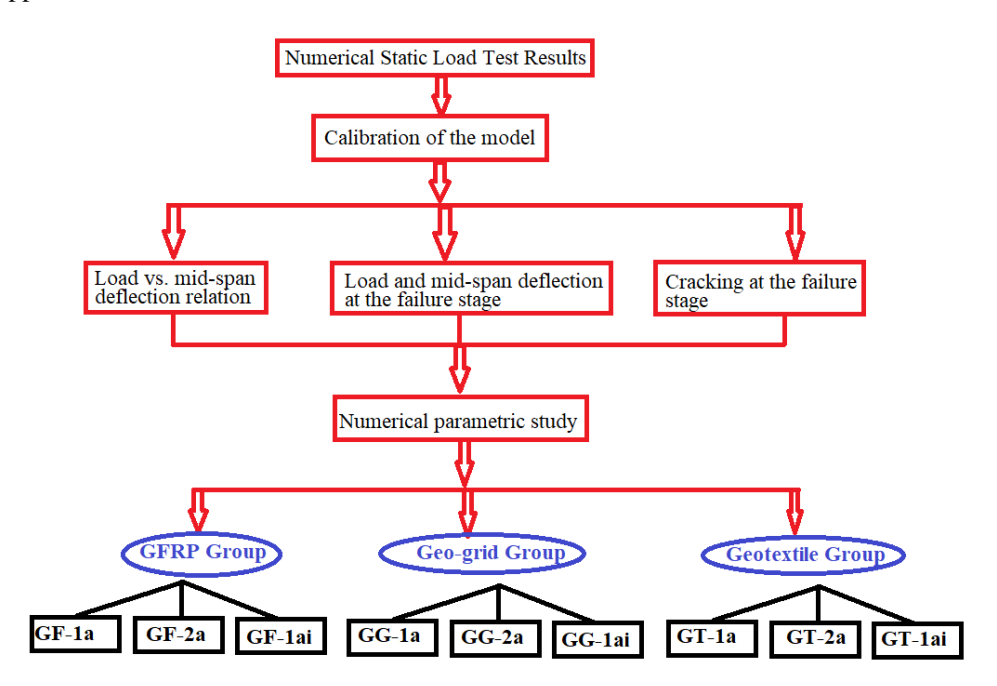


Figure 1. Flowchart for the research methodology

3. Test Specimens

The experimental program from Majumder & Saha (2021) [25] included testing 3 RC beams (with and without full wrapping mesh reinforcement) subjected to monotonic loads. The experimental procedure involves the casting of these beams with a cross-sectional size of 100 mm in width and 150 mm in height and a total length of 1050 mm. The main bars were 4 \emptyset mm. Figure 2 demonstrates the details of the evaluated specimens. Table 1 shows the findings of the concrete mix properties. Table 2 shows the steel bars' properties, while Table 3 shows the reinforcement mesh's properties.

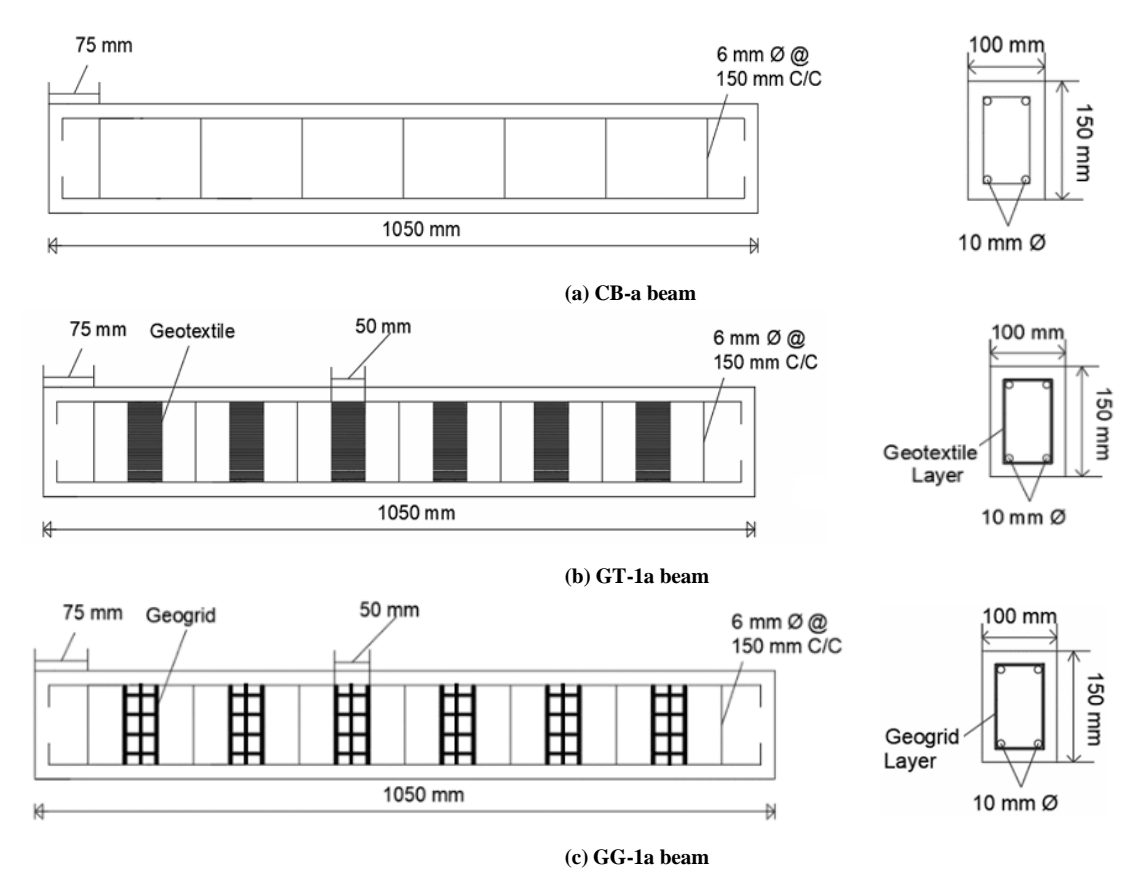


Figure 2. Details of adopted samples [25]

Table 1. Results of concrete mix [25]

 $\begin{array}{c} Cubic \ compressive \ strengths \\ f_{cu} \ (MPa) \end{array}$	Splitting tension strength (MPa)
27.5	3.1

Table 2. Test of steel bars [25]

Bar diameter (mm)	Area of cross-section (mm²)	fy (MPa)	fu (MPa)
6	28.3	387	490
10	78.5	445	570

Table 3. Properties of mesh reinforcement [25]

Material	Tensile Strength (kN/m)	Modulus-of elasticity (GPa)	Poisons Ratio	Thickness (mm)	Elong. at break (%)	Axial stiffness (kN/m)
Non-woven Geotextile	58	68	0.26	0.6	42	412
Uniaxial Geogrid	75	77	0.32	1.3	23	786

4. Modelling and Analysis of Tested Columns in ABAQUS

This study uses the Finite Element Method to analyze beams using the ABAQUS CAE version 2019 software [26], especially utilizing the Standard/Explicit Model. The structural analysis of all beams was performed utilizing a single-step method, specifically by static analysis. The concrete beams and steel plates were modeled with the isoperimetric eight-node brick element (C3D8R). The three-dimensional two-node bar element, exhibiting motion in the x, y, and z dimensions, referred to as the truss element (T3D2), was utilized for the reinforced steel bars.

Multiple methods were employed to depict the various forms of reinforcing mesh, resulting in the following conclusions: i- For soft reinforcement mesh characterized by small, closely spaced fibers, such as geotextile or soft GFRP mesh, representation is achieved by constructing a Shell-Homogenous section with the requisite thickness (S4R: A 4-node doubly bent shell, whether thin or thick, utilizing decreased integration, hourglass control, and accommodating finite membrane stresses, as illustrated in Figure 3. ii- For coarse reinforcement mesh featuring large cross-sections and widely spaced fibers, such as geogrid or coarse GFRP mesh, representation is accomplished by creating a shell-surface

section and subsequently defining the properties of the rebar layers in both directions (SFM3D4: A 4-node quadrilateral surface element), as depicted in Figure 4. To comprehensively analyze every sample inside the ABAQUS environmental framework, several components were created, as seen in Figure 5. The supports on the ends of the beam are modeled as simply supported. Figure 6 illustrates the boundary constraints and load specifications (displacement control).

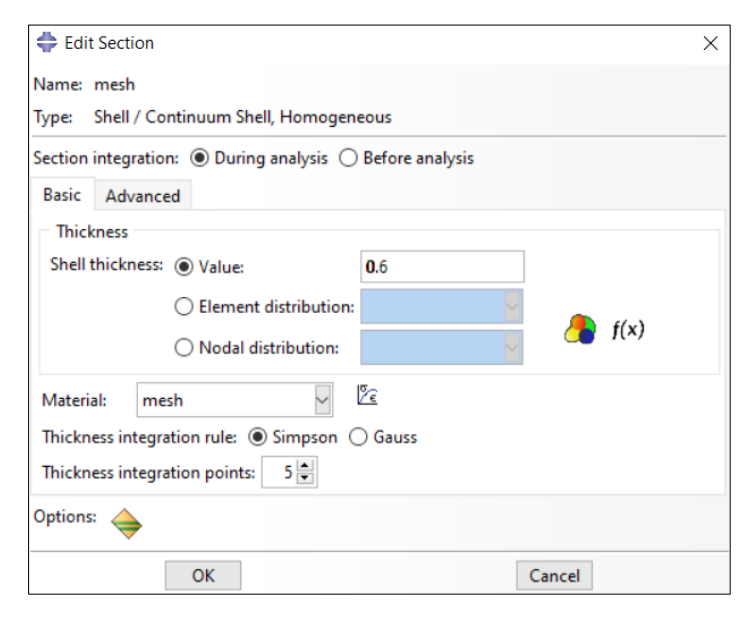


Figure 3. Representation of mesh by Shear-Homogeneous type

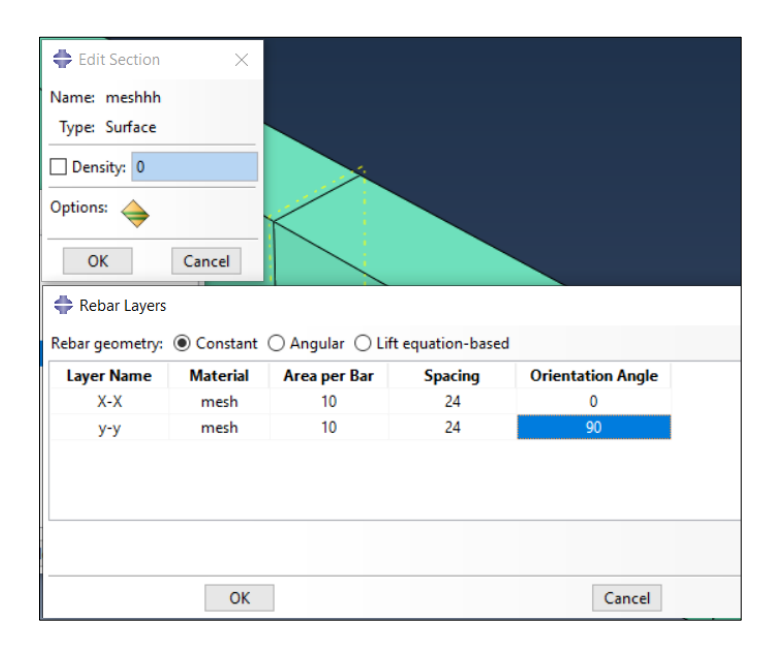


Figure 4. Representation of mesh by shell-surface- rebars type

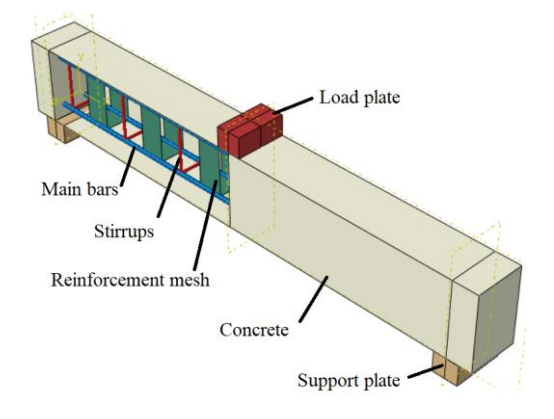


Figure 5. Creating parts and assemblies in ABAQUS

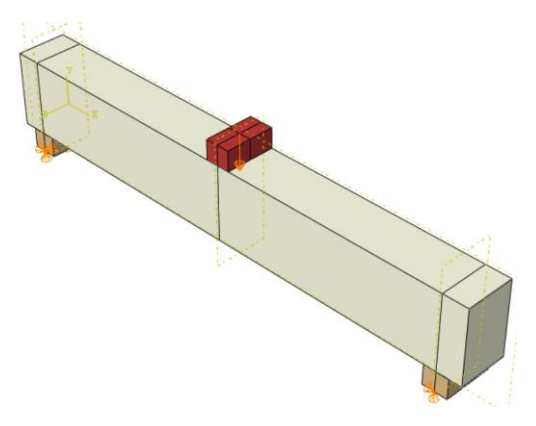


Figure 6. Conditions of boundaries and loads utilized in the analysis

For a thorough evaluation of interaction, the steel reinforcement and meshes are considered completely encased (embedded) in concrete. An interaction constraint of the Tie type was implemented between the concrete part and the steel plates of the load and supports. Refer to Figure 7. Table 4 demonstrates the input data for concrete damage plasticity. Tables 5 and 6 present the compressive and tensile results for mix1, respectively, from Majumder & Saha (2021) [25]. The properties of steel reinforcement and mesh were defined as shown in Tables 2 and 3.

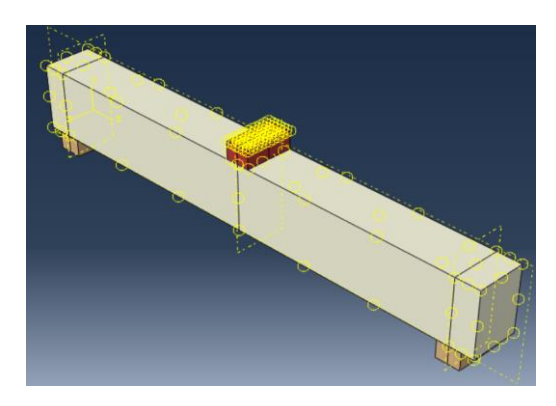


Figure 7. Interaction between parts

Table 4. Input information for concrete damage plasticity

Elasticity modulus (MPa)	Poisson' ratio	Dilation angle (degree)	Eccentricity	ϵ_{bo} / ϵ_{co}	Viscosity
22194	0.18	40	1.16	0.667	0

Table 5. Concrete compressive data

Yield Stress (MPa)	Inelastic Strain
8.258089581	0
12.7550867	9.49559E-05
16.48896216	0.000195652
19.28460212	0.000336837
21.14552368	0.000516755
22.18880165	0.000738138
22.3	0.000990762
21.68738692	0.001522212
19.81237039	0.002110316
17.59548849	0.002710754
15.43731163	0.003302559
13.4433903	0.003895997
11.71686531	0.00447444
6.312480439	0.007191854
3.797926686	0.009824644
2.517981169	0.012387056
1.791950027	0.014894622
1.331499412	0.017435276
1.028859186	0.019953851

Table 6. Concrete tension data

Yield Stress (MPa)	Strains
3.1	0
1.929692448	0.000146688
1.435796041	0.000266391
0.849593695	0.000589777
0.620528671	0.000898916
0.438983273	0.001406158
0.345041265	0.001909906
0.286811617	0.002412229
0.24684985	0.002913823
0.217561501	0.003414992
0.195083975	0.003915888
0.101097594	0.008919638
0.070822729	0.013920845
0.055407856	0.01892146
0.045931793	0.023921838
0.03946144	0.028922097
0.034735486	0.033922285
0.031117494	0.038922429

5. The Calibration of the Manufactured Finite Element Model

This section provides several comparisons of the experimental results and relevant numerical data. The aspects of interest include the relationships between load and mid-span deflection under external pressures, cracking at failure, and the assessment of load and mid-span deflection at the failure point.

5.1. Load vs. Mid-Span Deflection Relation

Figures 8 to 10 show comparisons in load vs mid-span deflection relation between the numerical and experimental findings for the beams. The computer models had more stiffness than the data from experiments in both the linear and nonlinear behavior, but an acceptable degree of concordance was observed between them. Some factors may increase FEM analysis stiffness. Certain factors may account for increased stiffness in FEM analysis outcomes. Microcracks induced by drying shrinkage and curing were seen in the concrete during the experiment. These would reduce the inherent stiffness of the specimen. The modelling of these microcracks is absent in finite element models. The link between concrete and bras in the FE analyses is presumed to be flawless. This assumption will not be entirely accurate for the actual specimen [27].

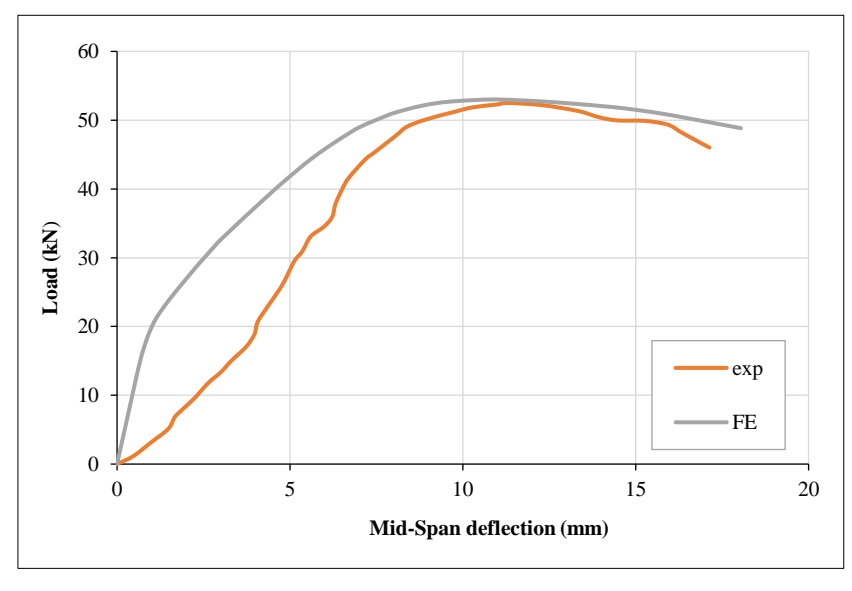


Figure 8. Numerical and experimental analysis of load against mid-span deflection of the CB-a beam

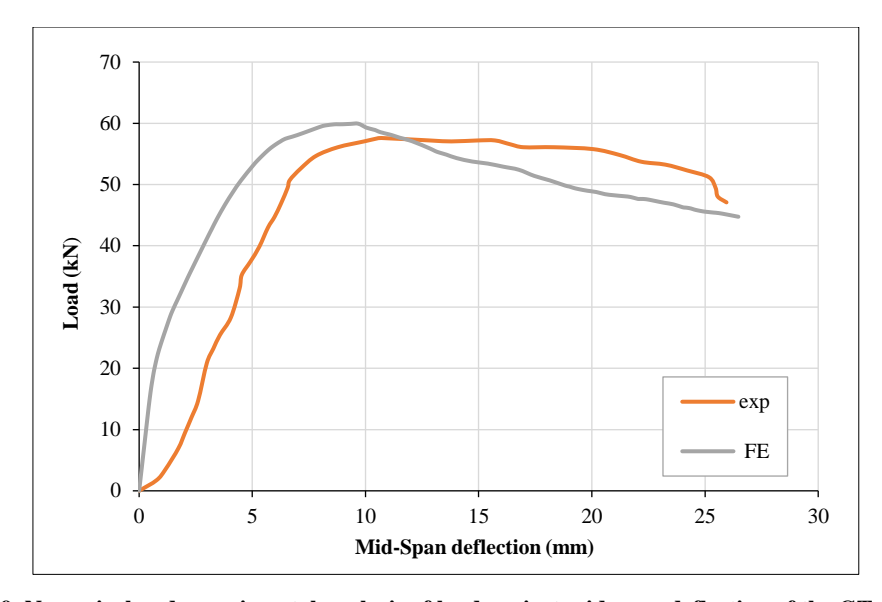


Figure 9. Numerical and experimental analysis of load against mid-span deflection of the GT-1a beam

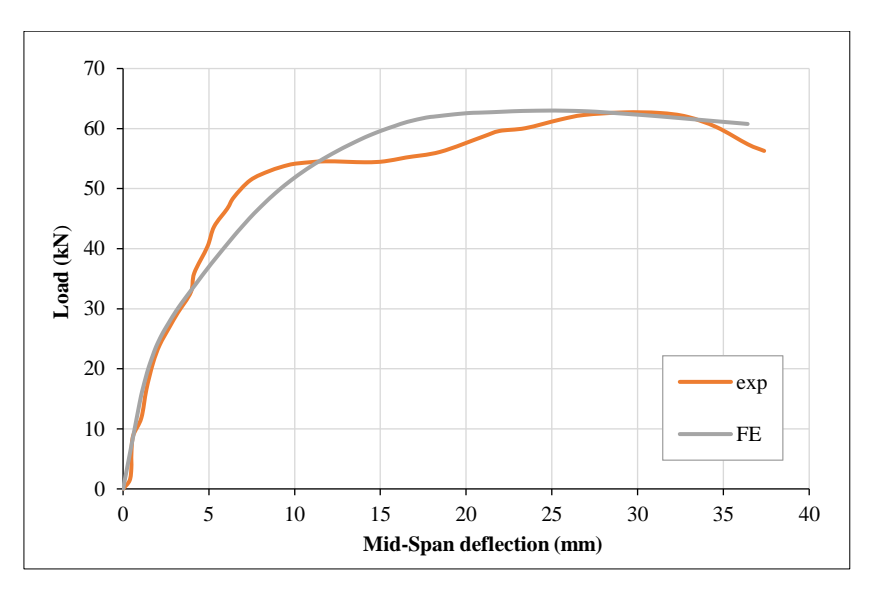


Figure 10. Numerical and experimental analysis of load against mid-span deflection of the GG-1a beam

5.2. Load and Mid-span Deflection at the Failure Stage

Table 7 presents a comprehensive comparison of the ultimate load and midspan deflection acquired from the numerical model and the experimental results carried out at the failure stage for all specimens. A robust connection was seen between the failure load and axial deflection values derived from FE models and those acquired from experimental tests, with the average and coefficient of variation for (Pu) FE/(Pu)Exp being 1.018 and 1.873%, respectively, for ultimate loads, while, for the mid-span deflection (Δu FE / Δu Exp) they were 0.902 and 5.462%, respectively.

Table 7. Experimental and numerical ultimate load and midspan deflection

Beam ID	Ultimate Load (Pu)			Axial deflection at ultimate load (Δu		
Beam ID	EXP(kN)	FE. (kN)	FE/EXP	EXP (mm)	FE. (mm)	FE/EXP
CB-a	52.5	53	1.0095	11.3	10.75	0.9513
GT-1a	57.6	59.9	1.0399	10.7	9.68	0.9046
GG-1a	62.7	63	1.0047	29.2	24.9	0.8527
	Average		1.018	Averag	ge	0.902
Sta	ndard deviatio	n	0.0191	standard de	viation	0.0493
Coefficient of variation (%)		1.873	Coefficient of variation (%)		5.462	

5.3. Cracking at the Failure Stage

The contour graphic in Figure 11 shows the maximum plastic main strain in the experimental beams and their fracture patterns in the final stage, showing how loads affect strain concentrations and crack patterns. The crack pattern matches numerical and experimental data.

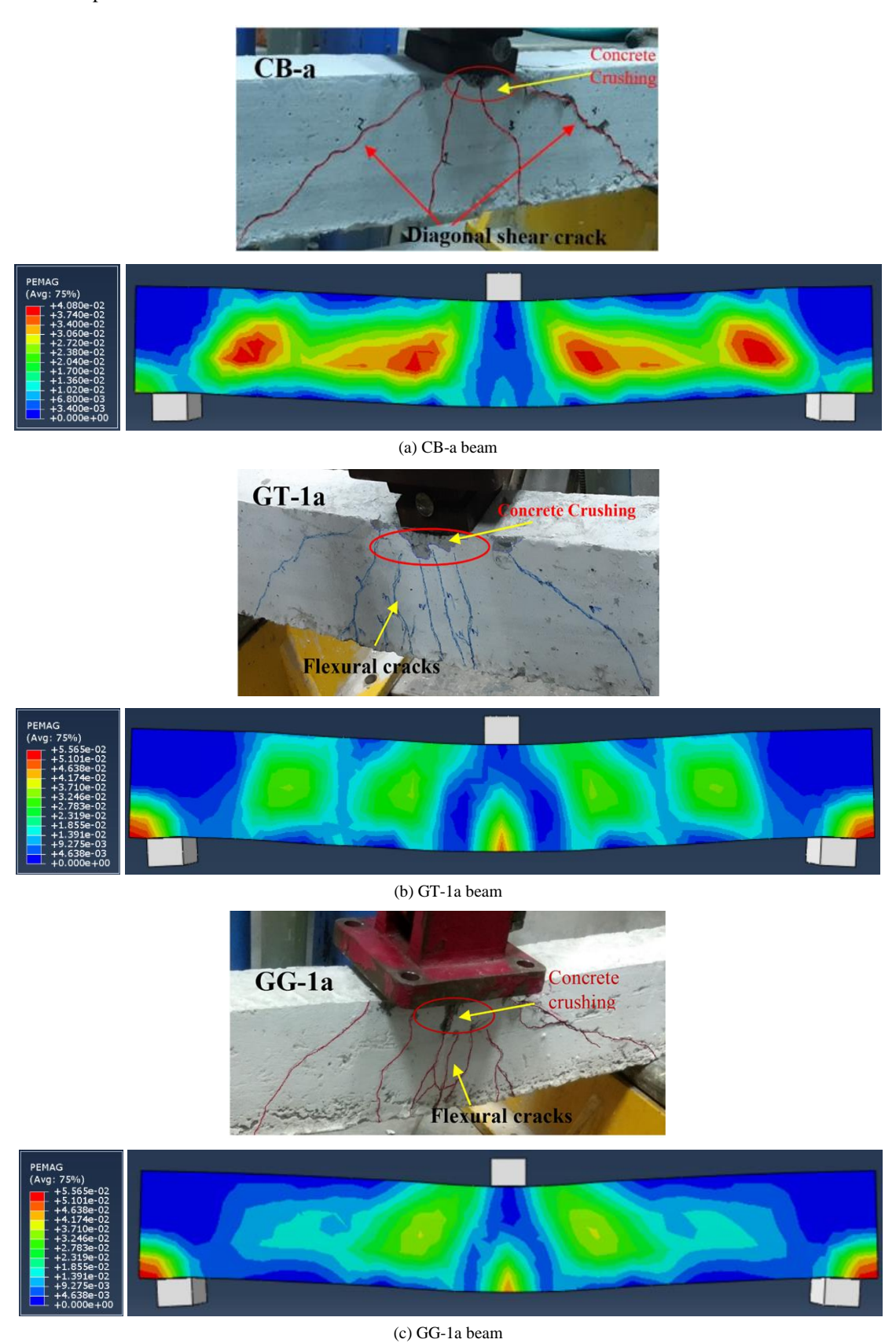


Figure 11. Ultimate damage outcome of numerical and experimental beams, experimental pictures from Hashemi et al. (2024) [20]

6. Numerical Parametric Study

In light of the preceding validation of the FE evaluation for the experimental data obtained in this study, a comprehensive parametric study was carried out using the FE model. The investigation parameters are:

- Material of reinforcement mesh (Non-woven Geotextile, Uniaxial Geogrid, or GFRP). Two old models, GT-1a and GG-1a, in addition to a new model with GFRP mesh (GF-1a), were used for this;
- Angle of inclination of mesh strip (90 or 45 °);
- The effect of mesh strip width or the number of mesh strips, keeping the same total width of all strips = 300mm.

Knowing that all specimens have the same old details of steel reinforcement and concrete. See Table 8 and Figure 12. Table 9 shows the properties of all meshes.

Table 8. Details of the parametric study beams

Group	Beam ID	Material of mesh	Number of mesh strips	Width of mesh strip (mm)	Angle of inclination (degree)
	GT-1a	Non-woven Geotextile	6	50	90
1	GG-1a	Uniaxial Geogrid	6	50	90
	GF-1a	GFRP	6	50	90
	GT-1ai	Non-woven Geotextile	6	50	45
2	GG-1ai	Uniaxial Geogrid	6	50	45
	GF-1ai	GFRP	6	50	45
	GT-2a	Non-woven Geotextile	4	75	90
3	GG-2a	Uniaxial Geogrid	4	75	90
	GF-2a	GFRP	4	75	90

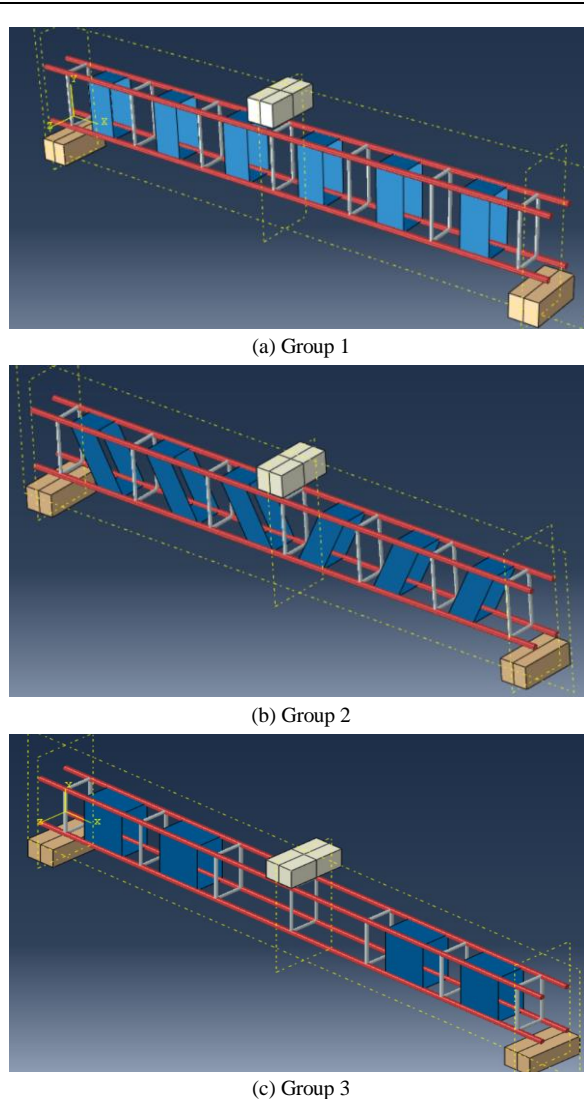


Figure 12. Creating parts and assembly of parametric study beams

Table 9. Properties of mesh reinforcement of the parametric study

Materials	Tensile Strengths (kN/m)	Modulus of elasticity (GPa)	Poisons Ratio	Thickness (mm)	Elong. at breaking (%)	Axial stiffness (kN/m)
Non-woven Geotextile*	58	68	0.26	0.6	42	412
Uniaxial Geogrid *	75	77	0.32	1.3	23	786
GFRP **	70	90	0.33	0.3	39	690

^{*} From reference [25], ** From reference [28].

6.1. Load vs. Mid-span Deflection Relation

The impact of reinforcement mesh material on the load vs axial deflection relationship is depicted in Figure 13. From load vs deflection relations, it is evident that all beams exhibit equal stiffness throughout the elastic range subsequent to the occurrence of cracking, except for the geotextile beam, which had higher stiffness. When approaching the ultimate load stage, the geogrid beam gave greater stiffness than the beam with GFRP.

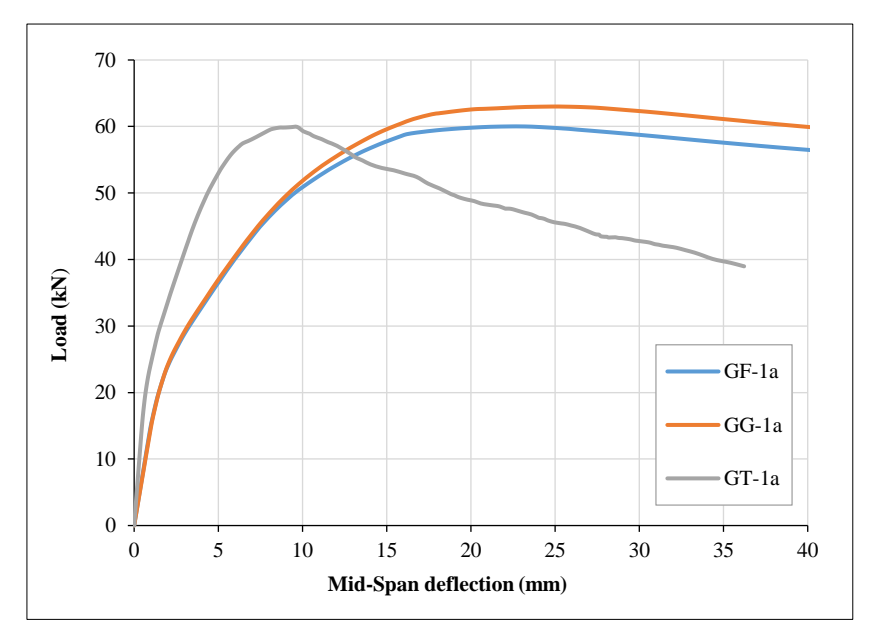
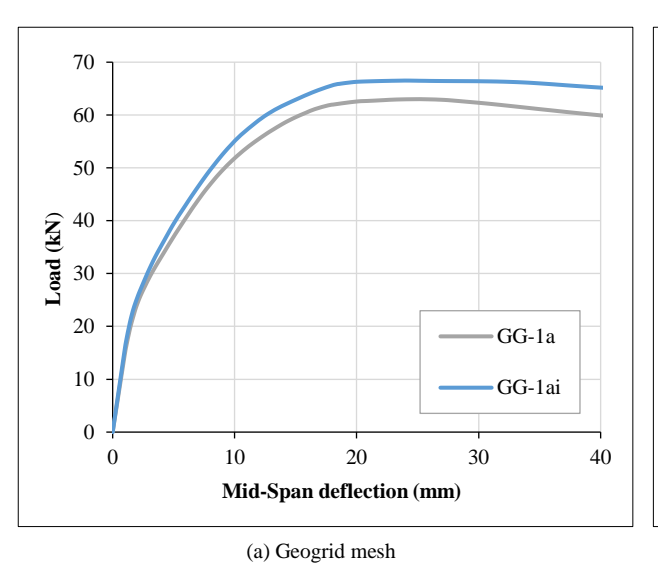
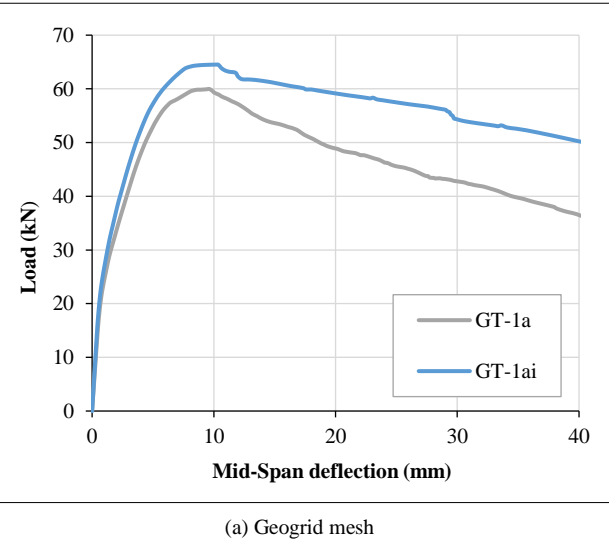


Figure 13. Effect of reinforcement mesh material on load vs mid-span deflection relationship

The impact of the angle of inclination of the mesh strip on the load vs axial deflection relationship is shown in Figure 14. From load vs deflection relations, it is evident that each of the two beams exhibits equal stiffness throughout the elastic range subsequent to the occurrence of cracking. When approaching the ultimate load stage, the inclined strip's beam gave higher stiffness than the vertical one.





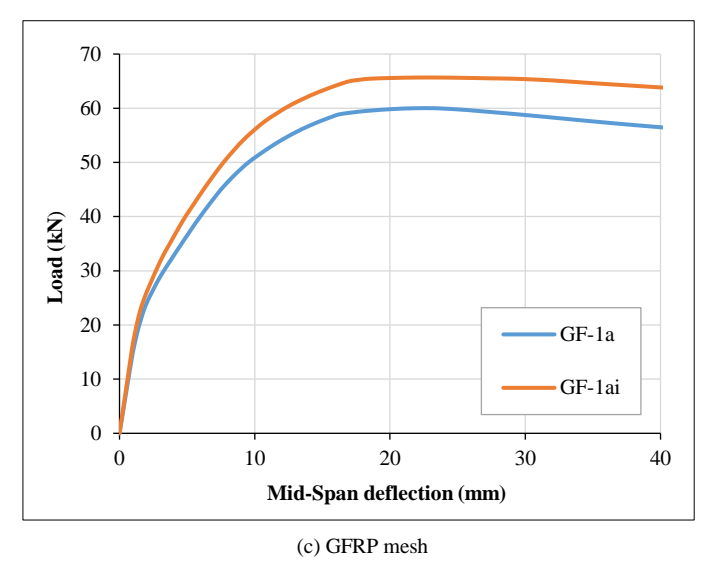


Figure 14. Impact of angle of inclination of mesh strip on load vs mid-span deflection relationship

The effect of mesh strip width or number of mesh strips on the load vs axial deflection relationship is demonstrated in Figure 15. From load vs deflection relations, it is evident that each of the two beams exhibits equal stiffness throughout the elastic range subsequent to the occurrence of cracking. When approaching the ultimate load stage, the beam with six strips (width of 50mm) gave higher stiffness than the beam with four strips (width of 75 mm).

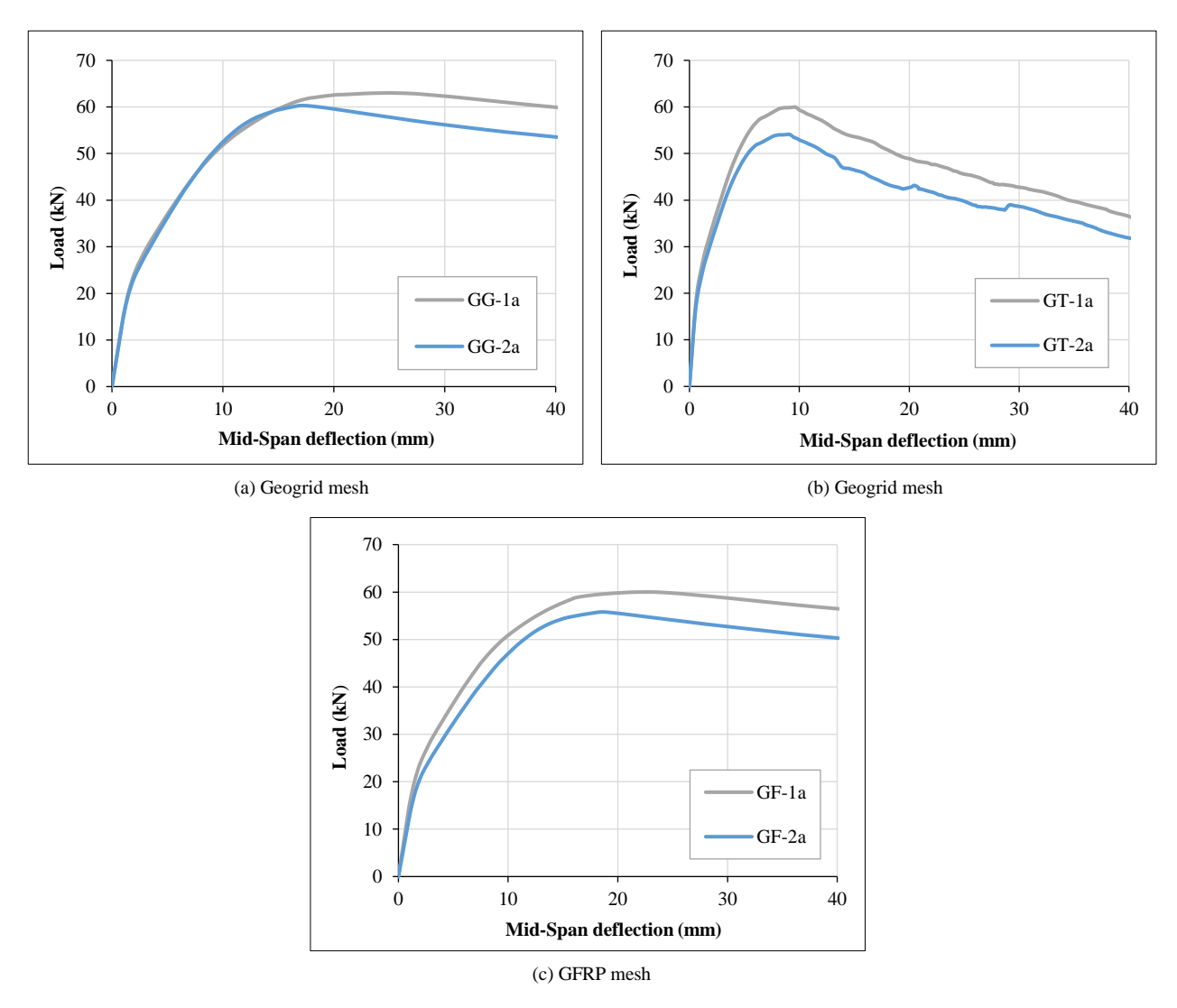


Figure 15. Impact of mesh strip width (number of strips) on load vs mid-span deflection relationship

6.2. Ultimate Load

Figure 16 and Table 10 show the impact of reinforcement mesh material upon the ultimate load. In general, for all groups, the geogrid beams gave the highest ultimate load and the geotextile beams gave the lowest ultimate load, as the percentage of decrease in the ultimate load value was (1.3 to 7.5%) and (4.9 to 10.3%) for the GFRP and geotextile beams, respectively, compared to the similar geogrid beams.

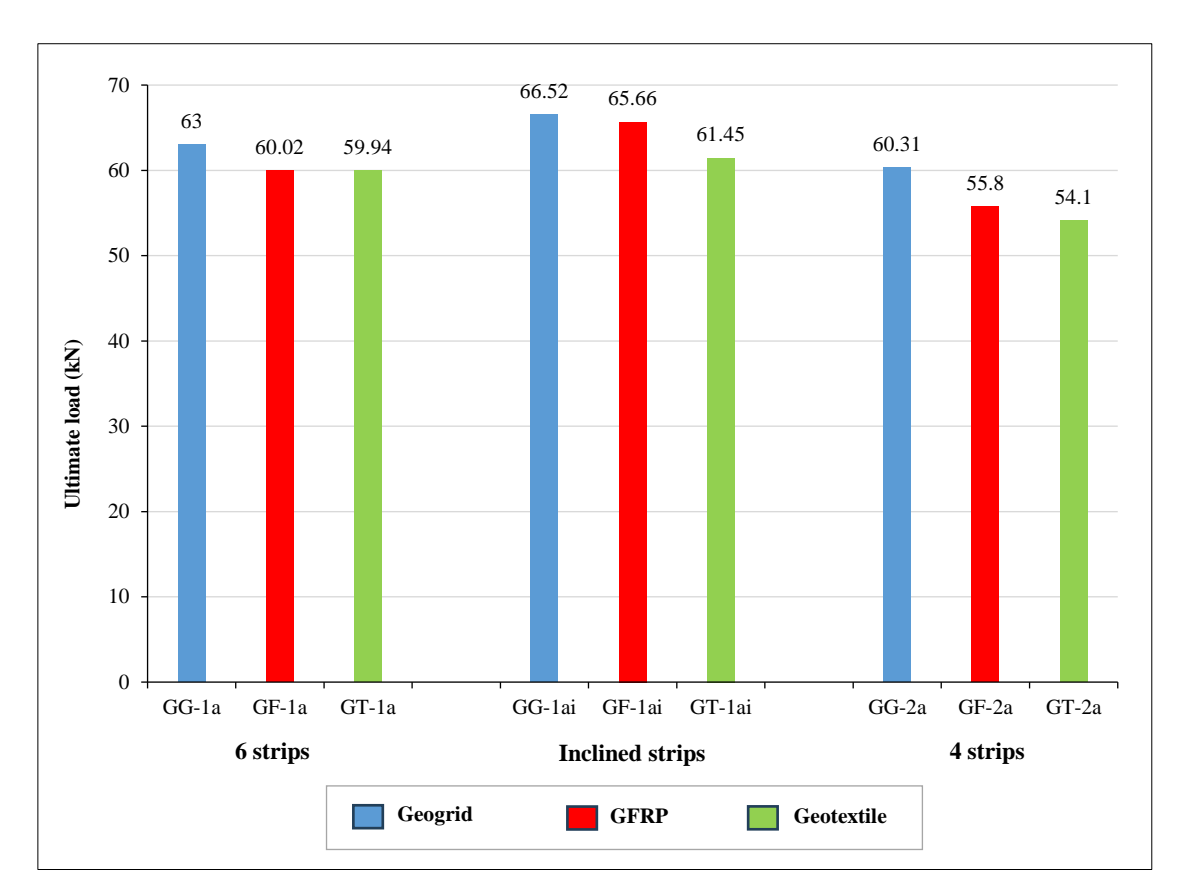


Figure 16. Impact of reinforcement mesh material on the ultimate load

Table 10. Effect of reinforcement mesh material on the ultimate load

Beam ID	Mid-span deflection @ Pu (mm)	Ultimate load Pu (kN)	Decrease percentage of Pu (%)
GG-1a	22.41	63	Ref.
GF-1a	23.28	60.02	4.7
GT-1a	9.67	59.94	4.9
GG-1ai	21.88	66.52	Ref.
GF-1ai	23.97	65.66	1.3
GT-1ai	10.33	61.45	7.6
GG-2a	18.75	60.31	Ref.
GF-2a	17.09	55.8	7.5
GT-2a	9.13	54.1	10.3

Figure 17 and Table 11 show the effect of the inclination of the mesh strip (90 or 45 °) upon the ultimate load. In general, for all groups, the inclined strip beams gave an ultimate load higher than the beams with vertical strips, where the ultimate load for beams with inclined strips was higher than that for beams with vertical strips by 5.6, 2.5, and 9.4% for beams with geogrid, geotextile, and GFRP mesh, respectively. This result supports the results of reference [29].

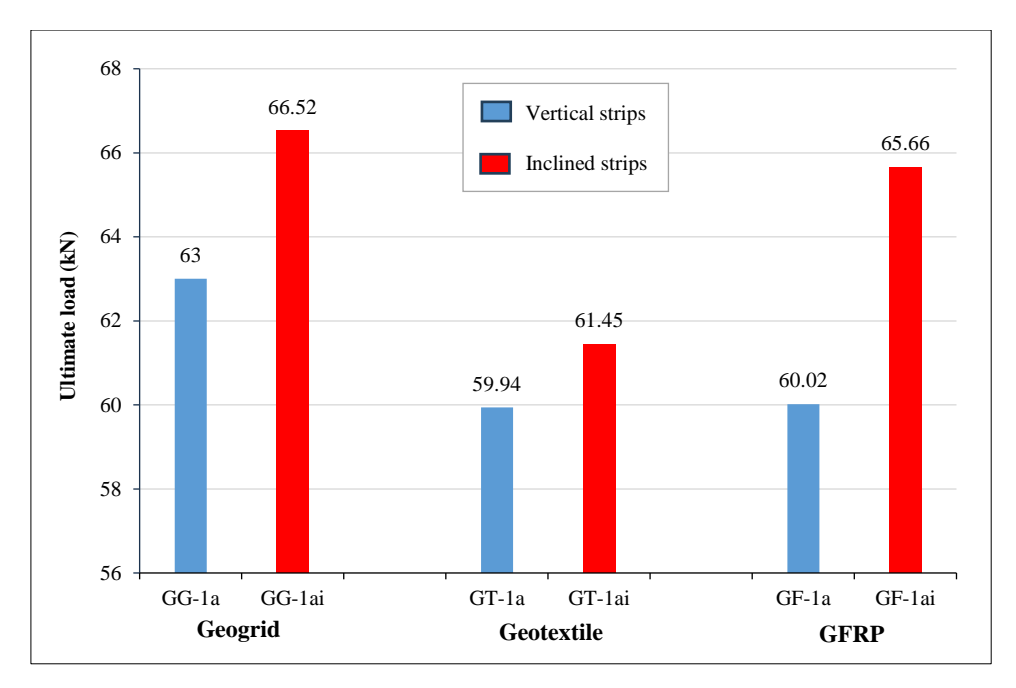


Figure 17. Impact of inclination of mesh strip on the ultimate load

Table 11. Effect of inclination of mesh strip on the ultimate load

Beam ID	Mid-span deflection @ Pu (mm)	Ultimate load Pu (kN)	Increase the percentage of Pu (%)
GG-1a	24.84	63	Ref.
GG-1ai	23.97	66.52	5.6
GT-1a	9.67	59.94	Ref.
GT-1ai	10.33	61.45	2.5
GF-1a	22.41	60.02	Ref.
GF-1ai	21.88	65.66	9.4

Figure 18 and Table 12 show the effect of mesh strip width or the number of mesh strips on the ultimate load. The ultimate load for beams with six strips (width of 50mm) was higher than that for beams with four strips (width of 75mm) by 4.3, 9.7, and 7% for beams with geogrid, geotextile, and GFRP mesh, respectively. This result supports the results of the reference [22].

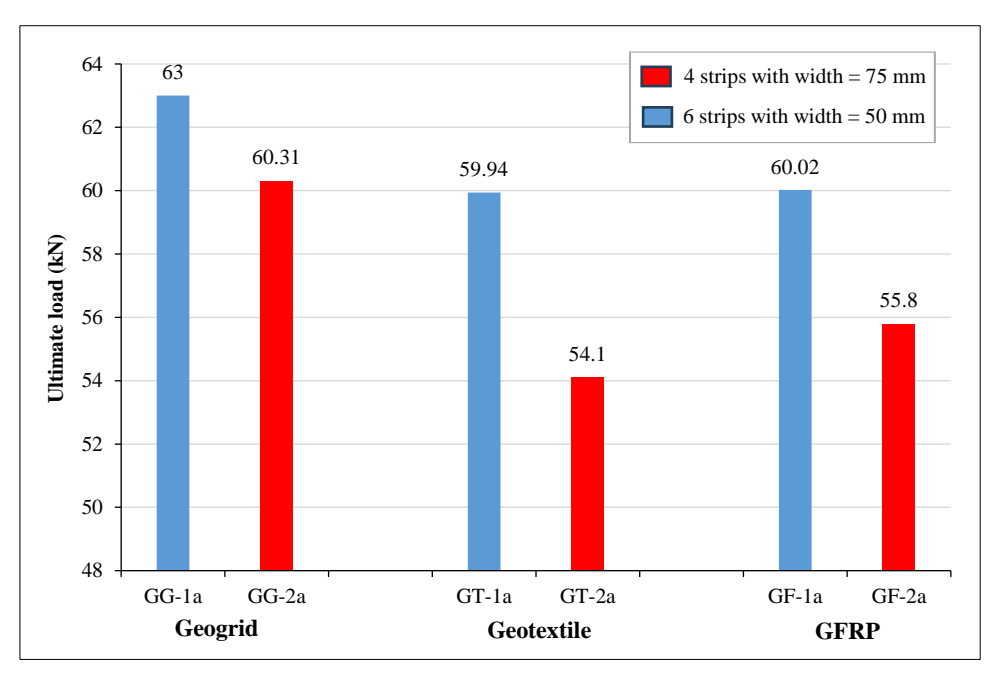


Figure 18. Impact of mesh strip width or number of mesh strips on the ultimate load

Table 12. Effect of mesh strip width or number of mesh strips on the ultimate load

Beam ID	Mid-span deflection @ Pu (mm)	Ultimate load Pu (kN)	Decrease percentage of Pu (%)
GG-1a	24.84	63	Ref.
GG-2a	17.09	60.31	4.3
GT-1a	9.67	59.94	Ref.
GT-2a	9.13	54.1	9.7
GF-1a	22.41	60.02	Ref.
GF-2a	18.75	55.8	7

6.3. Ductility Index

The ductility index quantifies a structural member's ability to endure significant deformations. The ratio of midspan deflections at failure loads over midspan deflection at the first yielding of tensile main bars. The yield deflection value was obtained by recording the value of deflection at the yield strain value of the lower steel bars at the mid-span. The ductility index increased with the addition of grid mesh; this result supports the results of reference [17]. Table 13 shows that: The effect of material type on the ductility index value was fluctuating and small, beams with inclined strips gave higher ductility indexes than similar beams with vertical strips, beams with beams with six strips (width of 50mm) gave higher ductility indexes than similar beams with four strips (width of 75mm).

Table 13. Effect of mesh strip width or number of mesh strips on the ultimate load

Beam ID	Yielding deflection (mm)	Ultimate deflection (mm)	Ductility factor (D.F.) = ultimate Def./ yield Def.
GG-1a	7.14	22.41	3.138
GF-1a	6.5	23.28	3.581
GT-1a	3.15	9.67	3.069
GG-1ai	6.8	21.88	3.217
GF-1ai	6.5	23.97	3.687
GT-1ai	2.71	10.33	3.811
GG-2a	6.56	18.75	2.858
GF-2a	7	17.09	2.441
GT-2a	3.1	9.13	2.945

6.4. Absorbed Energy

The absorbed energy is influenced by both the highest load value and the deflection at failure, since it is directly proportional to the area beneath the load-deflection curve. Table 14 presents the comprehensive energy measurements of the examined beams. It is clear that the beams with geotextile reinforcement meshes gave the lowest values of absorbed energy, and the reason for this is that they have the lowest values of ultimate load and deflections at ultimate load. When comparing similar beams in the type of mesh material, the beams with inclined strips gave the highest values of absorbed energy.

Table 14. Absorbed energy of beams

Group	Beam ID	Mid-span deflection @ Pu (mm)	Pu (kN)	Absorbed Energy (kN.mm)
1	GT-1a	9.67	59.94	448
	GG-1a	22.41	63	1238
	GF-1a	23.28	60.02	1056
2	GT-1ai	10.33	61.45	529
	GG-1ai	21.88	66.52	1253
	GF-1ai	23.97	65.66	1125
3	GT-2a	9.13	54.1	382
	GG-2a	18.75	60.31	752
	GF-2a	17.09	55.8	769

6.5. Stiffness of Beams at the Service Stage

Table 15 shows the stiffness at the service stage for all the beams. The chosen serviceability level was the experimental ultimate load divided by 1.70, as recommended by many researchers, such as Mansur et al. (1992) [30]. It is clear that the beams with geotextile reinforcement meshes gave the highest values of initial stiffness, and the reason for this is that the shape of the soft tissue and thus the appropriate method of representing it numerically, as we mentioned previously, gave results that are somewhat identical to the practical results. When comparing similar beams in the type of mesh material, the beams with inclined strips gave the highest values of stiffness.

				_	
Group	Beam ID	Ultimate Load Pu (kN)	Service Load (Ps=Pu/1.7) (kN)	Service Deflection (Ds) (mm)	Stiffness K=Ps/Ds (kN/mm)
1	GT-1a	59.94	35.3	2.2	16.05
	GG-1a	63	37.1	5.12	7.25
	GF-1a	60.02	35.3	4.7	7.51
2	GT-1ai	61.45	36.1	1.9	19
	GG-1ai	66.52	39.1	4.9	7.98
	GF-1ai	65.66	38.6	4.52	8.54
3	GT-2a	54.1	31.8	2.1	15.14
	GG-2a	60.31	35.5	4.5	7.89
	GF-2a	55.8	32.8	5.2	6.31

Table 15. Stiffness of beams at the service stage

6.6. Stresses in Reinforcement at the Ultimate Load Stage

Figures 19 to 27 show general profile values and distribution of the stresses in steel bars and meshes at the ultimate limit state.

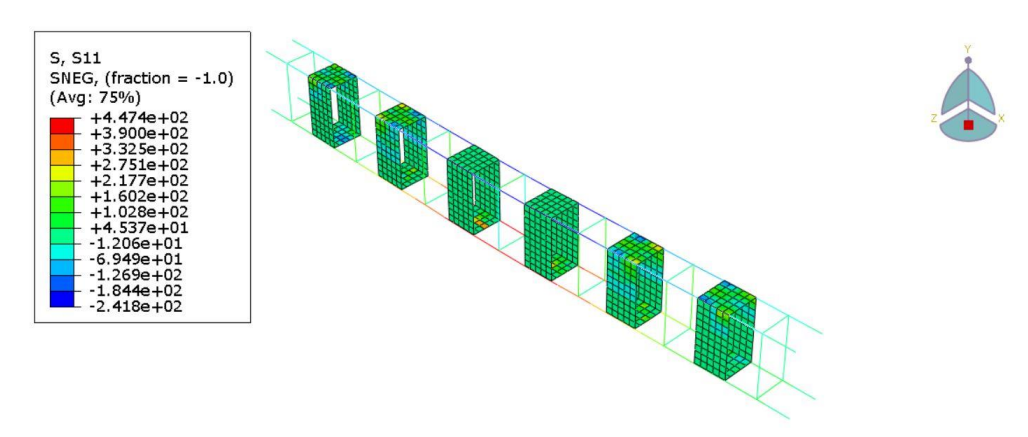


Figure 19. Distribution of the stresses in steel bars and meshes at the ultimate limit state for GF-1a

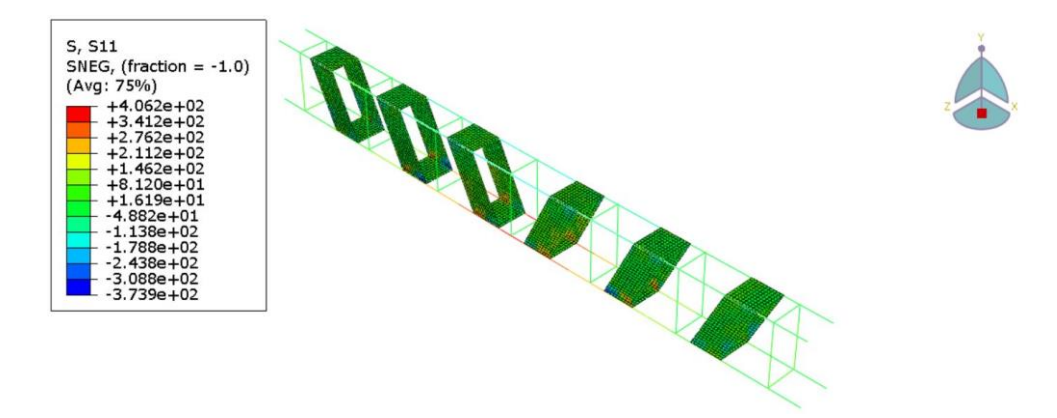


Figure 20. Distribution of the stresses in steel bars and meshes at the ultimate limit state for GF-1ai

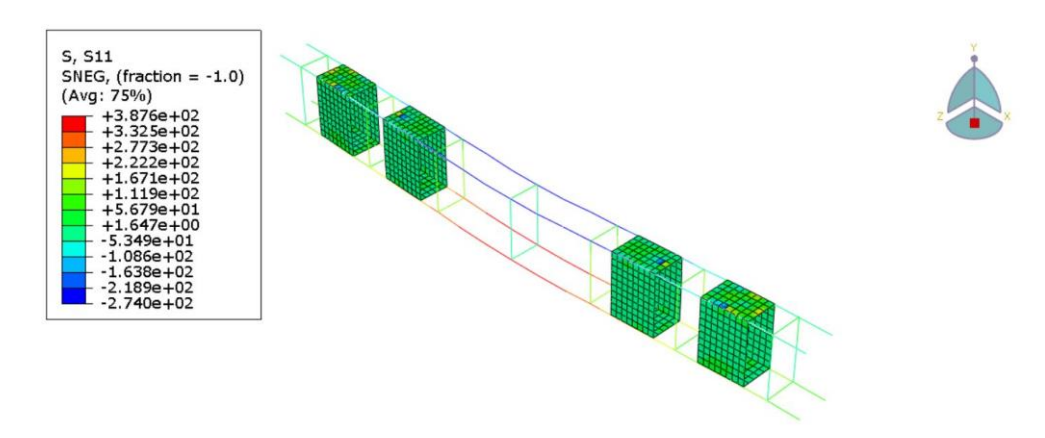


Figure 21. Distribution of the stresses in steel bars and meshes at the ultimate limit state for GF-2a

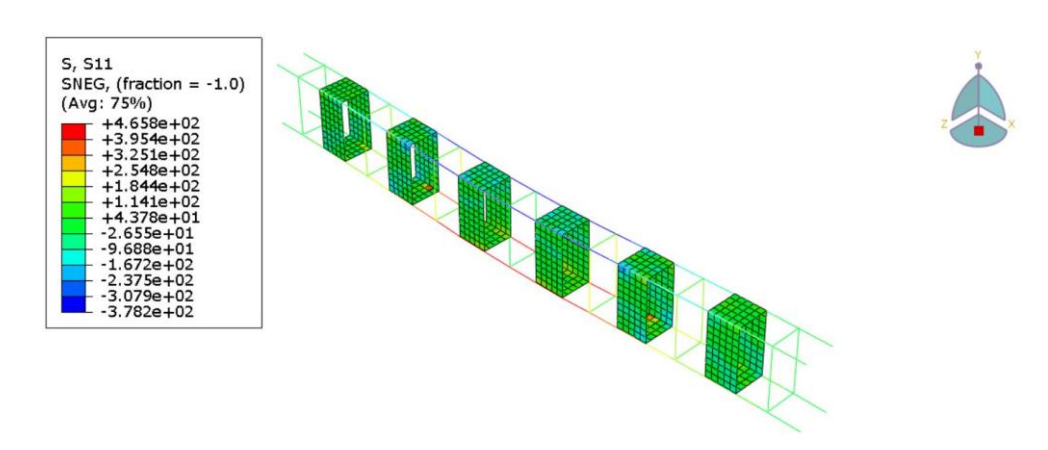


Figure 22. Distribution of the stresses in steel bars and meshes at the ultimate limit state for GG-1a

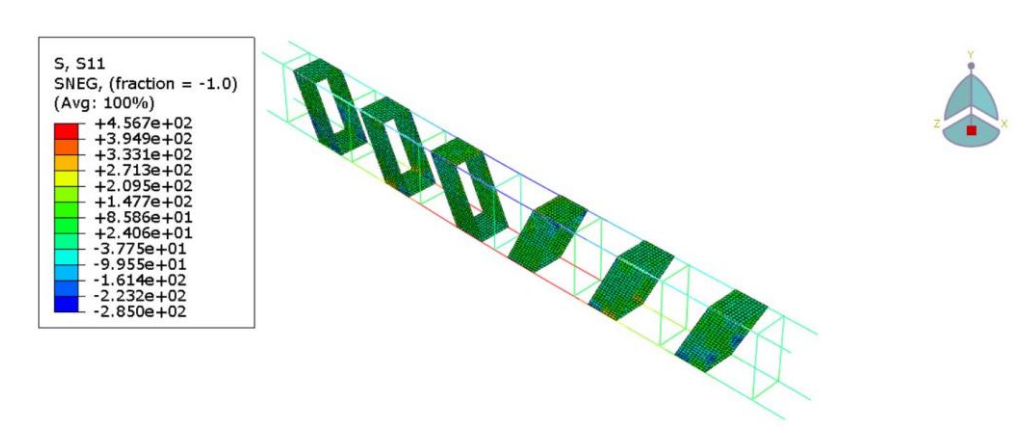


Figure 23. Distribution of the stresses in steel bars and meshes at the ultimate limit state for GG-1ai

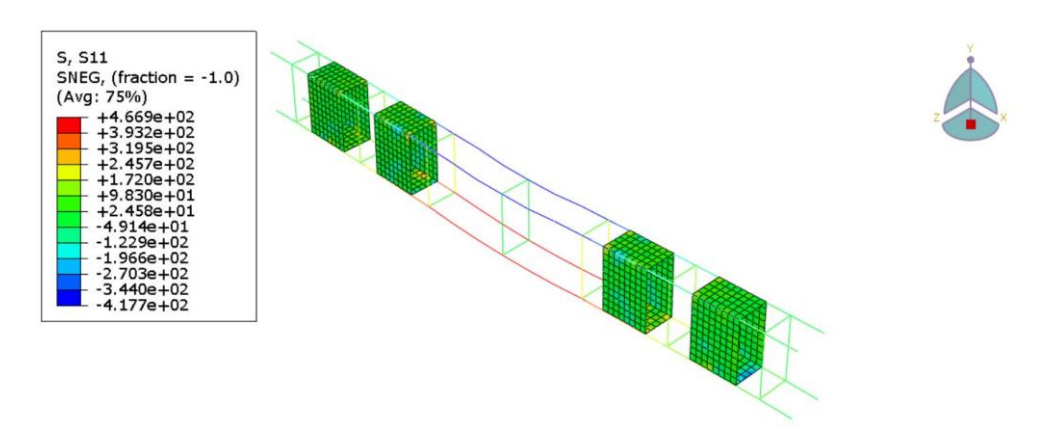


Figure 24. Distribution of the stresses in steel bars and meshes at the ultimate limit state for GG-2a

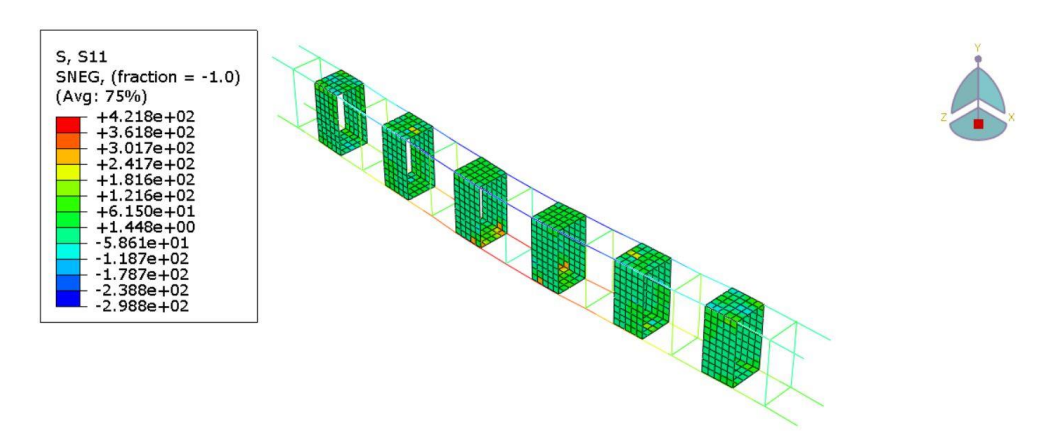


Figure 25. Distribution of the stresses in steel bars and meshes at the ultimate limit state for GT-1a

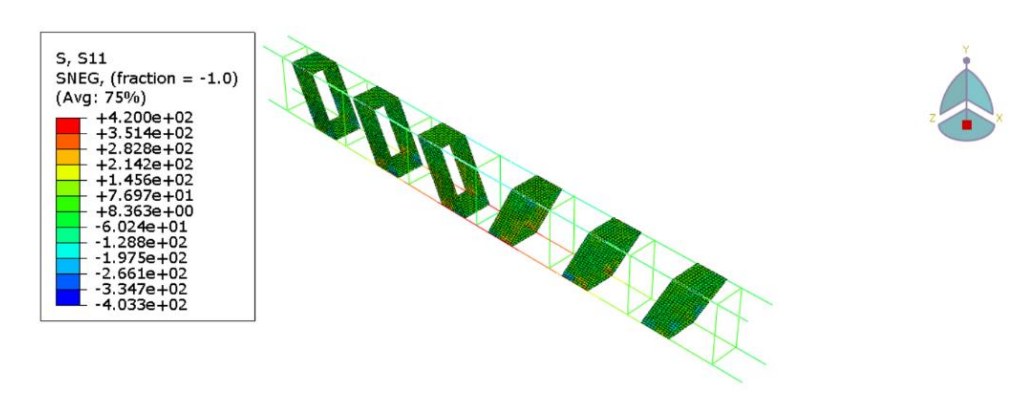


Figure 26. Distribution of the stresses in steel bars and meshes at the ultimate limit state for GT-1ai

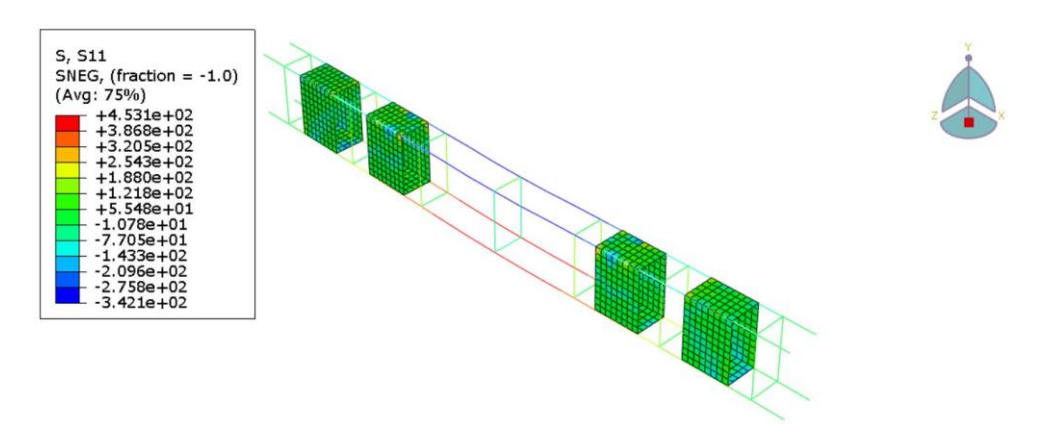


Figure 27. Distribution of the stresses in steel bars and meshes at the ultimate limit state for GT-2a

7. Conclusions

- A robust connection was seen between the failure load and midspan deflection values derived from FE models and
 those acquired from experimental tests, where the value of the average and coefficient of variation for
 (Pu)FE/(Pu)Exp were 1.018 and 1.873%, respectively, for ultimate loads, whilst for the mid-span deflection (Δu
 FE / Δu Exp) they were 0.902 and 5.462%, respectively.
- The geogrid beams gave the highest ultimate load, and the geotextile beams gave the lowest ultimate load, as the percentage of decrease in the ultimate load value was 1.3 to 7.5% and 4.9 to 10.3% for the GFRP and geotextile beams, respectively, compared to the similar geogrid beams.
- The inclined strip beams had ultimate loads higher than the beams with vertical strips, with the ultimate load for beams with inclined strips being higher than that for beams with vertical strips by 5.6, 2.5, and 9.4% for beams with geogrid, geotextile, and GFRP mesh, respectively.
- The ultimate load for beams with six strips (width of 50 mm) was higher than that for beams with four strips (width of 75 mm) by 4.3, 9.7, and 7% for beams with geogrid, geotextile, and GFRP mesh, respectively. That is, the smaller the strip width and the larger the number, the better.

• The effect of material type on the ductility index value fluctuated and was small. Beams with inclined strips (45°) gave higher ductility indexes than similar beams with vertical strips, and beams with six strips (width of 50 mm) gave higher ductility indexes than similar beams with four strips (width of 75 mm).

• Beams with geotextile reinforcement meshes gave the lowest values of absorbed energy because they have the lowest values of ultimate load and deflection at ultimate load. When comparing similar beams to the type of mesh material, the beams with inclined strips gave the highest value of absorbed energy.

8. Declarations

8.1. Author Contributions

Conceptualization, B.F.A., T.H.I., H.K.M., and A.A.A.; methodology, B.F.A., T.H.I., H.K.M., and A.A.A.; software, investigation, B.F.A., T.H.I., H.K.M., and A.A.A.; writing—original draft preparation, B.F.A., T.H.I., H.K.M., and A.A.A.; writing—review and editing, B.F.A., T.H.I., H.K.M., and A.A.A. All authors have read and agreed to the published version of the manuscript.

8.2. Data Availability Statement

The data presented in this study are available upon request from the corresponding author.

8.3. Funding

The authors received no financial support for the research, authorship and/or publication of this article.

8.4. Conflicts of Interest

The authors declare no conflict of interest.

9. References

- [1] Zhang, K., & Sun, Q. (2018). The use of Wire Mesh-Polyurethane Cement (WM-PUC) composite to strengthen RC T-beams under flexure. Journal of Building Engineering, 15(1), 122–136. doi:10.1016/j.jobe.2017.11.008.
- [2] Mebrahtom, M., Fissha, Y., Ali, M., Gebretsadik, A., Kide, Y., Nguse, Z., Gebrehiwot, Z., Flores, E. S., Avudaiappan, S., & Ikeda, H. (2024). Comparative study of eco-friendly wire mesh configurations to enhance sustainability in reinforced concrete structures. Scientific Reports, 14(1), 8818. doi:10.1038/s41598-024-59050-2.
- [3] Abdulkareem, B. F., Izzet, A. F., & Oukaili, N. (2021). Post-Fire Behavior of Non-Prismatic Beams with Multiple Rectangular Openings Monotonically Loaded. Engineering, Technology and Applied Science Research, 11(6), 7763–7769. doi:10.48084/etasr.4488.
- [4] Augustino, D. S. (2024). Shear Performance of Deep Concrete Beams with Openings Using Waste Tyre Steel Fibres: FEM and ANN Analysis. Civil Engineering Journal, 10(8), 2422–2449. doi:10.28991/CEJ-2024-010-08-02.
- [5] Abdulkareem, B., & Izzet, A. F. (2022). Serviceability of Post-fire RC Rafters with Openings of Different Sizes and Shapes. Journal of Engineering, 28(1), 19–32. doi:10.31026/j.eng.2022.01.02.
- [6] Mohammed, S. D., Salman, H. M., Ibrahim, T. H., Oukaili, N. K., & Allawi, A. A. (2025). On the Impact of Lacing Reinforcement Arrangement on Reinforced Concrete Deep Beams Performance. Civil Engineering Journal (Iran), 11(2), 726–745. doi:10.28991/CEJ-2025-011-02-019.
- [7] Allawi, A. A., & Ali, S. I. (2020). Flexural behavior of composite GFRP pultruded I-section beams under static and impact loading. Civil Engineering Journal (Iran), 6(11), 2143–2158. doi:10.28991/cej-2020-03091608.
- [8] Triantafillou, T. C. (1998). Shear strengthening of reinforced concrete beams using epoxy-bonded FRP composites. ACI Structural Journal, 95(2), 107–115. doi:10.14359/531.
- [9] Abdulkareem, B. F., & Izzet, A. F. (2022). Residual post fire strength of non-prismatic perforated beams. IOP Conference Series: Earth and Environmental Science, 961(1), 12002. doi:10.1088/1755-1315/961/1/012002.
- [10] Tetta, Z. C., Koutas, L. N., & Bournas, D. A. (2015). Textile-reinforced mortar (TRM) versus fiber-reinforced polymers (FRP) in shear strengthening of concrete beams. Composites Part B: Engineering, 77, 338–348. doi:10.1016/j.compositesb.2015.03.055.
- [11] Tetta, Z. C., Koutas, L. N., & Bournas, D. A. (2016). Shear strengthening of full-scale RC T-beams using textile-reinforced mortar and textile-based anchors. Composites Part B: Engineering, 95, 225–239. doi:10.1016/j.compositesb.2016.03.076.
- [12] Majumder, S., Nanda, R. P., & Saha, S. (2018). Experimental and numerical investigation of RC beam strengthened with geogrid confinement. Conference proceedings on 16th symposium on earthquake engineering (16SEE), 20-22 December, 2018, IIT Roorkee, India.

[13] Yalciner, H., Kumbasaroglu, A., & Ergun, U. (2018). Effects of Geo-grid and Conventional Stirrups on Reinforced Concrete Beams With Polypropylene Fibers. Structures, 13, 230–242. doi:10.1016/j.istruc.2018.01.003.

- [14] Erfan, A. M., & El-Sayed, T. A. (2019). Structural Shear Behavior of Composite Box Beams Using Advanced Innovated Materials. Journal of Engineering Research and Reports, 5(2), 1–14. doi:10.9734/jerr/2019/v5i216920.
- [15] Zhang, H. Y., Yan, J., Kodur, V., & Cao, L. (2019). Mechanical behavior of concrete beams shear strengthened with textile reinforced geopolymer mortar. Engineering Structures, 196, 109348. doi:10.1016/j.engstruct.2019.109348.
- [16] Li, W., Tang, S., Huang, Z., Yang, X., Shi, T., & Xing, F. (2020). Shear behavior of concrete beam reinforced in shear with carbon fiber-reinforced polymer mesh fabric (CFRP-MF) configuration. Engineering Structures, 218, 110828. doi:10.1016/j.engstruct.2020.110828.
- [17] Al-Bazoon, M., Jaafer, A., Haidar, H., & Dawood, A. (2022). Shear Strengthening of Reinforced Concrete Beam Using Wire Mesh–Epoxy Composite. Civil Engineering Journal (Iran), 8(6), 1205–1226. doi:10.28991/CEJ-2022-08-06-09.
- [18] Li, W., Tang, S., Huang, X., Liu, W., Yang, X., & Shi, T. (2022). Carbon fiber-reinforced polymer mesh fabric as shear reinforcement in reinforced concrete beams. Journal of Building Engineering, 53, 104433. doi:10.1016/j.jobe.2022.104433.
- [19] Yang, X., & Huang, J. Q. (2024). Shear Behaviour of RC Beams Strengthened using CFRP Grid-ECC/PMM Matrix Composites: An Experimental and Numerical Investigation. Journal of Advanced Concrete Technology, 22(1), 1–13. doi:10.3151/jact.22.1.
- [20] Hashemi, S. S., Rezaei, S., Matin, M., & Vaghefi, M. (2024). Experimental investigation on the compressive behaviour of concrete confined by glass fibre geogrid mesh. International Journal of Structural Engineering, 14(3), 252–270. doi:10.1504/IJSTRUCTE.2024.139776.
- [21] Guo, X., Zhang, Z., Sun, Q., & Tian, P. (2024). Numerical Analysis on Flexural Shear Behavior of Reinforced Concrete Beams Strengthened with Fiber-Reinforced Polymer Grid and Engineered Cement Composites. Buildings, 14(8), 2304. doi:10.3390/buildings14082304.
- [22] Huang, Z., Shen, J., Lin, B., Miao, X., & Cheng, Z. (2024). Experimental and numerical investigation on shear behavior of concrete beams reinforced with CFRP grid shear reinforcements. Composite Structures, 349–350, 118552. doi:10.1016/j.compstruct.2024.118552.
- [23] Kirthiga, R., & Elavenil, S. (2024). Performance evaluation of pre-damaged reinforced concrete beams strengthened with knitted glass fabric reinforced cementitious matrix: Flexure and shear behaviors. Structures, 70, 107744. doi:10.1016/j.istruc.2024.107744.
- [24] Zhang, Z., & Lan, J. (2025). Study on Shear Behavior of Reinforced Concrete Beams Strengthened with FRP Grid–PCM Composite Reinforcement. Applied Sciences, 15(11), 6103. doi:10.3390/app15116103.
- [25] Majumder, S., & Saha, S. (2021). Shear behaviour of RC beams strengthened using geosynthetic materials by external and internal confinement. Structures, 32, 1665–1678. doi:10.1016/j.istruc.2021.03.107.
- [26] ABAQUS. (2019) Analysis User's Manual, Version 6.14. Dassault Systemes Simulia, Inc., Providence, United States.
- [27] Kachlakev, D. I., Miller, T. H., Potisuk, T., Yim, S. C., & Chansawat, K. (2001). Finite element modeling of reinforced concrete structures strengthened with FRP laminates. No. FHWA-OR-RD-01-XX, Oregon Department of Transportation Research Group, Salem, United States.
- [28] Hanan, A. K., Muttashar, M. D., Abid, S. R., Yosri, A. M., Alsharari, F., & Deifalla, A. farouk. (2023). Flexural performance of concrete beams internally reinforced with steel, geogrid and GFRP meshes. Journal of Materials Research and Technology, 24, 9156–9170. doi:10.1016/j.jmrt.2023.05.146.
- [29] Al-Salloum, Y. A., Elsanadedy, H. M., Alsayed, S. H., & Iqbal, R. A. (2012). Experimental and Numerical Study for the Shear Strengthening of Reinforced Concrete Beams Using Textile-Reinforced Mortar. Journal of Composites for Construction, 16(1), 74–90. doi:10.1061/(asce)cc.1943-5614.0000239.
- [30] Mansur, M. A., Huang, L. M., Tan, K. H., & Lee, S. L. (1992). Deflections of reinforced concrete beams with web openings. ACI Structural Journal, 89(4), 391–397. doi:10.14359/3019.